

# Novel epoxy/cyclic olefin copolymer/carbon structural composites with electro-activated self-healing properties

Davide Perin  | Haroon Mahmood | Daniele Rigotti  | Andrea Dorigato | Alessandro Pegoretti 

Department of Industrial Engineering and INSTM Research Unit, University of Trento, Trento, Italy

## Correspondence

Davide Perin, Department of Industrial Engineering and INSTM Research Unit, University of Trento, Via Sommarive 9, Trento 38123, Italy.

Email: [davide.perin-1@unitn.it](mailto:davide.perin-1@unitn.it)

## Abstract

Multifunctional self-healing composites have great potential in several applications, i.e., from automotive to aerospace. This study examines the self-healing behavior of carbon fiber reinforced composites by depositing jet-spun cyclic olefin copolymer (COC) meshes on dry carbon fiber plies before lamination with epoxy resin (EP). Three different laminates were prepared, including neat EP/CF and two composites with 4 wt.% and 8 wt.% of COC in the form of a jet-spun network as a healing agent. The introduction of COC mesh reduced flexural stress by 26% and interlaminar shear strength by 50%. Mode I interlaminar fracture toughness ( $G_I$ ) was evaluated and specimens were mended at 110°C by resistive heating generated by an electrical current flowing within the samples. The laminates containing 8 wt% COC reported a healing efficiency, evaluated as the ratio between the  $G_I$  and as the ratio of the maximum load ( $P_{MAX}$ ) of virgin and healed samples, of 9.4% and 33.7%, respectively. Fractography analysis highlighted the poor adhesion between the COC mesh and EP matrix, and several COC microfibers were trapped inside the epoxy matrix, hindering their diffusion inside the crack zone, which limited the healing capability of the prepared laminates.

## KEYWORDS

carbon fibers, composites, cyclic olefin copolymers, fracture toughness, self-healing

## 1 | INTRODUCTION

In the recent years, polymer matrix composites (PMCs), and especially carbon fiber-reinforced plastics (CFRPs), have been among the fastest-growing materials for technical products thanks to their peculiar features such as elevated mechanical properties, lightness and environmental stability.<sup>1–3</sup> Due to the new CO<sub>2</sub> reduction targets and the urge for lightweight structures, the global demand for

composite materials in automotive, construction, and aerospace applications is forecasted to increase at a compound annual growth rate (CAGR) of approximately 6%. In this way, the total market will increase from \$26 billion in 2018 to \$41.4 billion in 2025.<sup>4,5</sup>

Despite all the benefits provided by the use of composite materials, a significant challenge still exists in predicting and monitoring their durability.<sup>6,7</sup> Interfacial delamination and/or matrix cracking are the typical

This is an open access article under the terms of the [Creative Commons Attribution-NonCommercial-NoDerivs](https://creativecommons.org/licenses/by-nc-nd/4.0/) License, which permits use and distribution in any medium, provided the original work is properly cited, the use is non-commercial and no modifications or adaptations are made.

© 2023 The Authors. *Polymer Composites* published by Wiley Periodicals LLC on behalf of Society of Plastics Engineers.

failure mechanisms of PMCs, but one of the heaviest limitations for these materials is the failure caused by fatigue crack propagation during service.<sup>8,9</sup> Repairing operations are usually labor-intensive, expensive, time-consuming, and with little to no effectiveness. Furthermore, the recycling operations of PMCs are complex.<sup>10</sup> For these reasons, among the scientific communities and the industrial world, a steadily increasing interest in a new generation of multifunctional composites possessing self-healing properties.<sup>11,12</sup> The use of self-healing composites could lead to several advantages, i.e., minimization of costs correlated to maintenance and repair operations, prolonged service life, and thus improved environmental sustainability, and decrease in the probability of uncontrolled failure.<sup>13,14</sup> To increase the effectiveness of the self-healing process in PMCs, four concepts must be taken into consideration: localization, time, repair mechanism, and mobility.<sup>15</sup> The concept of localization is linked to the types of damage in the composite, i.e., scratches, micro or macro cracks, delamination, and fiber debonding. The time interval between the occurrence of damage and its subsequent repair is closely associated with the second concept, i.e., time, the repairing time or operation is desirable to be minimized. The study of the healing mechanism is critical, an increase in the mobility of the healing agent inside the damaged region can strongly reduce the repairing time.

Self-healing composite materials are usually classified into extrinsic and intrinsic systems.<sup>16</sup> In extrinsic systems, the self-healing ability is activated autonomously,<sup>17</sup> while in intrinsic systems, the self-healing process must be triggered through the use of external stimuli, such as temperature, voltage, and magnetic field.<sup>18</sup> In extrinsic self-healing composites, the healing agent is usually contained in capsules<sup>19,20,21</sup>, vascular networks,<sup>22</sup> or nanoparticles, and has to be incorporated into the materials during the production of the composites.<sup>23</sup> When cracks occur within the material as a result of a damage event, the capsule or vascular network breakage allows the release of the healing agent into the damaged area. Through capillary action, the healing agent, together with the catalyst that triggers the polymerization of the healing agent, fills the crack area and restores the structural integrity of the material.<sup>24</sup> The extrinsic healing agent must possess suitable properties, such as good stability, flowability, and fast chemical reactivity for enabling quick healing.<sup>25</sup> The major drawbacks are the inherent decrease in the mechanical properties of the composite and the fact that the healing process can be performed one time only. In intrinsic self-healing composites, the material itself can restore micro damages through the inherent reversibility of bonding in the matrix.<sup>26</sup> The reversibility of the bonding enables to perform multiple healing cycles, which is a

great advantage in comparison to the extrinsic mechanism. Moreover, the intrinsic self-healing mechanisms rely on various factors, i.e., chain mobility, entanglement, and melting behavior of the thermoplastic phases.<sup>27</sup>

One method largely employed in literature for intrinsic self-healing composites is the introduction of thermoplastic polymers in epoxy resin. Michaud and Cohades have widely investigated epoxy/poly( $\epsilon$ -caprolactone) (PCL) systems, to obtain an optimal combination of toughness and stiffness.<sup>28–30</sup> They found that efficient healing is reliant on the presence of a continuous PCL phase capable to flow into cracks, even if an elevated PCL content leads to a worsening of both strength and toughness. Nevertheless, in an epoxy system containing 25 vol% of PCL, they recovered 70–80% of the initial fracture toughness upon a thermal mending process at 150°C for 30 min. Meure et al.<sup>31</sup> have investigated the self-healing properties of an epoxy/ethylene-methacrylic acid copolymer (EMAA) system. In their work, they processed EMAA via continuous fiber extrusion into a fiber mesh, which was subsequently utilized to develop a carbon fiber-reinforced epoxy composite.<sup>31</sup> They also inserted EMAA particles in epoxy-based composites to impart self-healing properties. In both cases, the thermal mending process was performed at 150°C for 30 min, and healing efficiency values above 100% were obtained. Mahmood et al.<sup>32,33</sup> embedded 20 and 30 wt% of cyclic olefin copolymer (COC) particles in an epoxy resin. They found that the fracture toughness increased upon COC addition, and they obtained healing efficiency values up to 80% after a thermal mending at 145°C for samples with a COC amount of 30 wt%. On the other hand, even though the dispersion of a thermoplastic powder inside the epoxy matrix was quite homogenous, it led to a noticeable increase in the viscosity of the uncured matrix, leading to processing difficulties. Thus, in order to improve the production process of the composites, several researchers have focused their attention on placing the healing agent directly on carbon fiber (CF) plies. In the work of Yao et al.,<sup>34</sup> they successfully electrospun a PCL mesh to prepare self-healing and shape memory epoxy/PCL matrices. The self-healing properties provided by the introduction of 14 wt% PCL were determined by comparing the tensile stress of virgin and healed specimens, and healing efficiency of 45% was observed. Cescato et al.<sup>35</sup> produced a porous electrospun mesh of PCL directly onto CF plies, to prepare structural epoxy self-healing composites. In their work, they achieved healing efficiency values up to 32% with a very limited PCL concentration (10 wt%). Wang et al.<sup>36</sup> successfully prepared a core-shell nanofiber self-healing composites by encapsulating epoxy resin and curing agent in

polyacrylonitrile by using coaxial electrospinning, to form two-component core-shell nanofibers. The healing efficiency of this system after a thermal mending at 120°C of 1 h was above 100%. In another work on self-healing composites performed by Costan Zovi et al.,<sup>37</sup> an impermeable thin film of COC was incorporated in the interlaminar region of epoxy/CF composites. The resulting laminates were characterized by an elevated healing efficacy (up to 100%), but a rather poor interlaminar adhesion due to the weak fiber/matrix interface.

The most widely used approach for producing microfibers is the electrospinning process, which relies on the electrostatic force required to spin fibers from a polymer solution droplet from a capillary.<sup>38</sup> However, the jet-spinning process offers several advantages over the electrospinning methods for producing microfibers, i.e., no use of voltage and/or elevated temperatures, and no hazardous solvents. Padron et al.<sup>39</sup> performed an extensive study concerning the production of nanofibers through force spinning. They were able, through their lab-made device, to produce microfibers of polyethylene oxide (PEO) at a rate 50 times higher than that obtained with single-needle electrospinning.

Based on these considerations, this work aims to develop intrinsic self-healing carbon fiber composites in which the self-healing functionality is provided by the presence of jet-spun COC microfibers directly deposited on CF plies. The presence of a porous mesh of COC could enable to maintain high workability of the uncured resin and also a satisfactory interfacial adhesion. Furthermore, the deposition through jet spinning is significantly faster than the electrospinning deposition and thus, this process enables to obtain higher yield and productivity. The produced composites were thoroughly characterized from the microstructural and thermo-mechanical characterization point of view. Concerning the mending operations, they were performed exploiting the Joule heating effect, thanks to the application of an electrical voltage. The healing efficiency of the prepared laminates was determined by comparing the interlaminar fracture toughness and the maximum load of virgin and healed samples. Fractography analyses were then thoroughly

performed in order to better understand the healing mechanism in the prepared laminates.

## 2 | MATERIALS AND METHODS

### 2.1 | Materials

The selected thermosetting matrix was an epoxy resin bi-component system, produced by Elantas Europe S.r.l. (Collecchio, Italy). This system was composed of an epoxy resin (Elantech EC 157.1) and an aminic hardener (Elantech W342), and the mixed ratio used was 100:30. Unidirectional CF fabrics (GV-201 U TFX), purchased from Angeloni S.r.l. (Venice, Italy), were used as reinforcing elements. These fibers were composed of high-strength CF plies with a surface density of 200 g/m<sup>2</sup> and thermoplastic-coated glass yarns (weft direction, density of 17 g/m<sup>2</sup>). The healing agent selected was TOPAS COC 9506F-500, provided by TOPAS Advanced Polymers GmbH (Raunheim, Germany) in the pellets form (density = 1.01 g/cm<sup>3</sup>, glass transition temperature = 65 °C, norbornene content = 61 wt%).

### 2.2 | Sample preparation

#### 2.2.1 | Jet-spinning of COC fibers

The deposition of COC on one side of CF fabrics was performed by a jet-spinning technique through a lab-made apparatus, shown in Figure 1. To produce a spinning dope, COC was dissolved in p-xylene at a concentration equal to 0.15 g/mL. The obtained solution was stirred for 1 h at room temperature until complete dissolution of COC and then transferred in a 10 mL glass syringe. Afterward, the syringe was mounted on a Harvard Apparatus Model 11 (Harvard Apparatus Inc., Holliston, MA, USA), equipped with a three-way needle. One extremity of the needle was connected to a nitrogen flow of 200 mL/min and the other to the syringe. Subsequently, the whole syringe pump apparatus was installed on an Arduino®-controlled slider, moving at a speed of 1 m/min along the

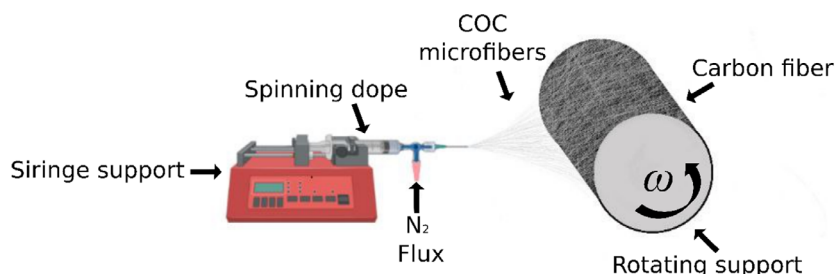


FIGURE 1 Schematic representation of the device used for the jet-spinning process.

Sample	CF Layers	COC Layers	COC content (wt%)	Thickness (mm)
EP-CF	6	5	—	1.3
EP-4COC_CF	6	5	4.6	1.5
EP-8COC_CF	6	5	7.6	1.3
EP-CF	18	17	—	3.4
EP-4COC_CF	18	17	4.8	3.7
EP-8COC_CF	18	17	8.2	4.0
EP-CF	30	29	—	5.1
EP-4COC_CF	30	29	4.5	6.0
EP-8COC_CF	30	29	7.7	6.3

TABLE 1 List of the prepared laminates.

axis of the collector cylinder. A collector drum covered with the CF ply, having a diameter of 25 cm and rotating at a speed of 60 rpm, was fixed at a distance of 15 cm from the tip of the needle.

After an optimization of the jet-spinning process, five different COC concentrations were used to deposit meshes on CF plies, labeled as xCOC ( $x = 5, 10, 15, 20, 30, 40$ ), where  $x$  stands for the ml of spinning dope spun on top of the CF plies. After a comprehensive characterization of the COC spun meshes on CF plies, two different COC concentrations were further investigated and utilized for the composites preparation, i.e., 15COC and 30COC. The produced CF plies coated with COC were cut into plies having a width of 15 cm and length of 25 cm, for the preparation of the laminates, and then treated at 50°C for 7 days in vacuum to evaporate all the remaining p-xylene inside the produced fibers.

### 2.2.2 | Preparation of the composites

Composites were manufactured by combining two different fabrication techniques together, i.e., hand lay-up and vacuum-assisted resin transfer molding (VARTM). The combination of these two techniques was necessary to achieve the complete permeation of the resin within the laminates and to reduce the voids concentration as much as possible. In order to preserve the integrity of the spun COC mesh, the use of an optimized curing process was necessary. It was composed of a cycle of 8 h at room temperature and 15 h at 60°C performed under a pressure of 0.8 MPa in a Carver 2699 hot press (Carver Inc., Wabash, IN, USA). By using this manufacturing process, laminates with six-layers, eighteen-layers, and thirty-layers of neat epoxy/CF and composites having a nominal COC concentration equal to 4 wt% and 8 wt% were produced (the COC content in the laminates was determined through TGA tests, see Paragraph 3.1). These two concentrations in the laminates were obtained utilizing 15COC and

30COC plies, respectively. The six-layered laminates were used for the flexural tests and also for the electrical resistivity measurements, while the thirty-layered composites were utilized in short beam shear strength tests for the evaluation of the interlaminar shear strength (ILSS). Eighteen layered composites were used for the evaluation of the interlaminar fracture toughness. The specimens for these tests were prepared by inserting a polytetrafluoroethylene (PTFE) film 25  $\mu\text{m}$  thick on one side in the middle section of each sample, following ASTM D5528<sup>40</sup> standard. Table 1 reports the list of the prepared laminates, together with their relative composition and thickness.

## 2.3 | Experimental techniques

### 2.3.1 | Characterization of the COC spun meshes on CF plies

TGA tests were carried out on the COC spun meshes using a TG50 MT5 (Mettler-Toledo, Columbus, OH, USA) thermobalance, with a nitrogen flow of 100 mL/min and a heating rate of 10°C/min from 30°C to 700°C. At least 6 specimens were tested for each deposition. Field emission scanning electron microscope (FESEM) images of the jet-spun meshes on CF plies were obtained through a Supra 40 (Carl Zeiss AG, Oberkochen, Germany) microscope after Pt-Pd sputtering. The distributions of the diameters of the obtained COC microfibers were obtained from image segmentation analysis by using the ImageJ 1.52 software.<sup>41</sup> In order to assess the thermal stability of the produced microfibers, a thermal treatment emulating the curing cycle of the epoxy resin was performed. Thus, the microfibers were kept for 8 h at room temperature and 15 h at 60°C. The morphological analysis through FESEM demonstrated that the morphology and diameter of the fibers were not affected by the thermal treatment, meaning that the curing cycle on the composites did not affect the morphology of the healing agent inside the laminates.

### 2.3.2 | Characterization of the laminates

The microstructure of the prepared composites was investigated through an Axiophot optical microscope (Carl Zeiss AG, Oberkochen, Germany), equipped with a Leica DC300 digital camera (Leica Microsystems Ltd., Heerbrugg, Switzerland). The laminates were incorporated in epoxy resin and cured for 24 h at room temperature. Subsequently, the obtained samples were polished by using abrasive grinding paper made of silicon carbide with grit polishing sizes of 500, 800, 1200, and 4000, sequentially, and then polished with 3  $\mu\text{m}$  and 1  $\mu\text{m}$  cloths.

FESEM analysis was performed to analyze the morphology of COC microfibers on the crack propagation surfaces of virgin and healed samples (for the details of the healing process see Paragraph 2.3.3). All the specimens were coated with a platinum/palladium alloy (Pt/Pd 80:20) coating for 20 s and observed with a Supra 40 microscope (Carl Zeiss AG, Oberkochen, Germany).

Density measurements on the produced laminates were performed according to the ASTM D792<sup>42</sup> standard, and thus the laminates were weighed in air and in ethanol. The measurements were carried out at 23°C by using a ME104 (Mettler-Toledo, Columbus, OH, USA) precision balance, having a sensitivity of  $10^{-4}$  g. In order to evaluate the volume fraction of voids, information regarding the density of the COC mesh and CF was necessary. These measurements were performed in an AccuPyc 1330 (Micromeritics, Norcross, GA, USA) helium pycnometer, equipped with a chamber of 1  $\text{cm}^3$ , in which 30 runs for each measurement were performed. The calculation of the experimental density ( $\rho_{exp}$ ) was performed with the expression reported in Equation (1):

$$\rho_{exp} = \frac{\omega_{air}}{\omega_{air} - \omega_{eth}} (\rho_{eth}) \quad (1)$$

where  $\omega_{air}$  and  $\omega_{eth}$  are the weight of the samples immersed in air and ethanol, respectively, while  $\rho_{eth}$  is the density of ethanol. The theoretical density of the composites ( $\rho_t$ ) was evaluated with Equation (2):

$$\rho_t = \frac{1}{\frac{\omega_M}{\rho_M} + \frac{\omega_{CF}}{\rho_{CF}} + \frac{\omega_{COC}}{\rho_{COC}}} \quad (2)$$

where  $\omega_M$ ,  $\omega_{CF}$ , and  $\omega_{COC}$  are the weight fractions of the matrix, carbon fibers, and COC, respectively, while  $\rho_M$ ,  $\rho_{CF}$ , and  $\rho_{COC}$  are the density of the constituents. For all the samples  $\rho_{CF}$  was equal to 1.74  $\text{g}/\text{cm}^3$ ,  $\rho_M$  to 1.23  $\text{g}/\text{cm}^3$ , and  $\rho_{COC}$  to 1.01  $\text{g}/\text{cm}^3$ . The volume fraction of voids ( $V_v$ ) was evaluated as reported in Equation (3):

$$V_v = \frac{\rho_t - \rho_{exp}}{\rho_t} \quad (3)$$

In order to determine the thermal stability of the produced composites, thermogravimetric analysis (TGA) was conducted by using a Mettler TG50IR thermobalance (Mettler Toledo Inc., Columbus, OH, USA). A total mass of 20 mg for each specimen was tested at a heating rate of 10°C/min from 35°C up to 700°C, under a nitrogen flow of 100 mL/min. In this way, it was possible to determine the temperature associated with a mass loss of 1% ( $T_{1\%}$ ), and 5% ( $T_{5\%}$ ). Furthermore, it was also possible to determine the temperature associated to the maximum mass loss rate ( $T_D$ ) of both COC and the epoxy matrix, considered as the peak of the mass loss derivative (DTG) curves and the residual mass at 700°C ( $m_{700}$ ).

The evaluation of the flexural properties of the produced composites was performed following the ASTM D790<sup>43</sup> standard. Three-point flexural tests were performed using an Instron<sup>®</sup> 5969 (Instron, Norwood, MA, USA) universal testing machine, equipped with a 50 kN load cell. Rectangular specimens having a thickness of 1.6 mm and a width of 12.7 mm were utilized. As reported in the standard, a span-to-depth ratio of 60:1 was set for the flexural modulus measurements, whereas a ratio of 40:1 was set for the determination of flexural strength, and a strain rate on the outer surface of the samples equal to 0.01  $\text{mm}^{-1}$  was utilized. At least 8 specimens were tested for each composition. Flexural stress at break ( $\sigma_f$ ) and flexural strain at break ( $\epsilon_f$ ) were calculated according to Equations (4) and (5).

$$\sigma_f = \frac{3 \cdot P_{max} \cdot L}{2 \cdot b \cdot d^2} \quad (4)$$

$$\epsilon_f = \frac{6 \cdot D \cdot d}{L^2} \quad (5)$$

where  $P_{max}$  is the maximum load on the load-deflection curve, L is the support span, b is the width of the beam tested, d is the depth of the beam tested, and D is the maximum deflection of the center of the beam.

Short beam shear strength test was performed in order to evaluate the interlaminar shear strength (ILSS) of the prepared laminates, according to ASTM D2344<sup>44</sup> standard. The samples were tested with an Instron<sup>®</sup> 5969 testing machine equipped with a 50 kN load cell, at a crosshead speed of 1 mm/min. At least ten specimens were tested for each composition and a span-to-length ratio equal to 4:1 was adopted. Equation (6) was used for the ILSS calculation:

$$ILSS = 0.75 \cdot \frac{P_m}{b \cdot h} \quad (6)$$

where  $P_m$  is the maximum load,  $L$  is the length of the specimen,  $b$  is the width of the sample, and  $h$  refers to the thickness of the specimen.

The interlaminar fracture toughness ( $G_I$ ) was evaluated according to ASTM D5528-21<sup>40</sup> standard and the samples were tested with an Instron<sup>®</sup> 5969 testing machine equipped with a 50 kN load cell. Double cantilever beam (DCB) specimens, 150 mm long and 25 mm wide, were cut from 18 layered laminates. The tests were performed with a crosshead speed of 2.5 mm/min for the loading phase, while the unloading stage was performed at 25 mm/min, according to the standard, and at least twelve specimens were tested for each composition. A digital webcam B910HD (Logitech, Lausanne, Switzerland) was utilized to monitor the crack propagation ( $a$ ) during the test. The Mode I interlaminar fracture toughness ( $G_I$ ) was then calculated by using Equation (7):

$$G_I = \frac{m \cdot P_c \cdot \delta_c \cdot F}{2 \cdot b \cdot a \cdot N} \quad (7)$$

where  $m$  is the slope of the  $\log(C/N)$  versus  $\log(a)$  curve,  $P_c$  is the critical force for mode I fracture,  $\delta_c$  is the critical load point displacement for mode I fracture,  $F$  is the large displacement correction factor,  $b$  is the width of the DCB specimen, and  $N$  is the large displacement and loading block correction factor.

The evaluation of interlaminar fracture toughness was performed considering the point where the load-displacement curve started to deviate from linearity (NL).

The tested DCB specimens were subjected to a healing process (see Paragraph 2.3.3) and tested again, to obtain the interlaminar fracture toughness of healed samples ( $G_{I-H}$ ). Thus, the healing efficiency ( $\eta_{GI}$ ) was evaluated as the ratio between the  $G_I$  values of the virgin ( $G_{I-V}$ ) and the healed samples, using the expression reported in Equation (8):

$$\eta_{GI} = \frac{G_{I-H}}{G_{I-V}} * 100 \quad (8)$$

Furthermore, the healing efficiency was also evaluated considering the maximum load reached by the virgin specimen ( $P_{\max-V}$ ) and by the healed specimen ( $P_{\max-H}$ ) during the interlaminar fracture toughness tests. In this case, the healing efficiency ( $\eta_{P_{MAX}}$ ) was evaluated using the expression reported in Equation (9):

$$\eta_{P_{MAX}} = \frac{P_{MAX-H}}{P_{MAX-V}} * 100 \quad (9)$$

### 2.3.3 | Healing process of the composites

Considering that the healing process was based on the Joule heating effect, the measurement of the resistivity of samples was of utmost importance. Thus, resistivity measurements were performed on the prepared composites by adopting a four-probe configuration following the ASTM D4496<sup>45</sup> standard. The tested specimens had a length of 40 mm, a width of 12.5 mm and were obtained from six layered laminates. DC electricity generator IPS 303DD (ISO-TECH Kunststoff GmbH, Ahaus, Germany) and two digital multimeters IDM 67 (ISO-TECH Kunststoff GmbH, Ahaus, Germany) were used for the measurements. The current passing through the samples was recorded at a voltage ranging from 0.5 V to 180 V. At least five specimens were tested for each composition. In this way, the volume resistivity ( $\rho_v$ ) and the surface resistivity ( $\rho_s$ ) of the samples were determined by using Equations (10) and (11), respectively:

$$\rho_v = \frac{V \cdot w \cdot t}{I \cdot l'} \quad (10)$$

$$\rho_s = \frac{V \cdot w}{I \cdot l'} \quad (11)$$

where  $V$  is the applied voltage,  $I$  is the applied current,  $w$  is the width,  $t$  is the thickness, and  $l'$  is the distance between the voltage electrodes, equal to 3.69 mm.

The Joule heating effect was used to activate the healing of the laminates, and it was applied through a lab-made device, which was composed of two steel electrodes covered with copper plates. According to a previous paper of our group,<sup>37</sup> a pressure of 500 kPa was applied through a torque wrench to repair the crack. To minimize the heat losses through the iron vice, a thin slab of polyurethane was inserted between each side of the vice and the specimen. A schematic representation of the lab-made device can be found in the previous work of our group.<sup>35</sup>

In order to apply the voltage and current to the specimens, a 6674A DC (Agilent Technologies, Inc., Santa Clara, CA, USA) generator was used. The voltage and the current were manually set to obtain a temperature of approximately 100°C on the crack surface for 30 min, as suggested in the literature for similar systems.<sup>46</sup> The surface temperature of the system was monitored during the



FIGURE 2 Representative thermal camera image of the EP\_4COC\_CF sample during the healing process.

repairing operation by using an infrared thermal camera E6 (FLIR Systems S.r.l., Limbiate, Italy). Figure 2 reports a representative image showing the temperature profile during the healing of the EP\_4COC\_CF sample. From this image, it is possible to notice that the temperature at the contact point of the electrodes was slightly higher ( $115^{\circ}\text{C}$ ), whereas, in the central zone, the temperature was slightly lower than  $100^{\circ}\text{C}$ .

### 3 | RESULTS AND DISCUSSIONS

#### 3.1 | Characterization of the COC spun meshes on CF plies

In order to assess the concentration of COC deposited on CF plies during the jet-spinning process, TGA analysis was performed. Figure 3 reports the representative TGA curves of neat CF, 5COC, 10COC, 15COC, 20COC, 30COC, and 40COC samples. It is possible to notice that neat carbon fibers present a limited weight loss at approximately  $400^{\circ}\text{C}$  most probably due to the degradation of the sizing agent. No solvent evaporation can be detected at  $140^{\circ}\text{C}$  (temperature corresponding to the boiling point of p-xylene), meaning that no traces of p-xylene can be found on the deposited plies. As could be expected, by increasing the COC deposition volume, it is possible to see that the resulting weight percentage of COC tends to increase, i.e., passing from  $1.2 \pm 0.2$  wt% for 5COC to  $10.4 \pm 1.0$  wt% for 30COC. On the other hand, by increasing the deposited volume above 30 mL, it is possible to see a decrease in the COC concentration down to  $9.6 \pm 0.7$  wt%. During the jet-spinning process, it was noticed that for COC volumes above 30 mL, the spun solution was deflected rather than deposited on the

carbon fiber fabric, without any additional COC deposition. According to this experimental evidence, a deposition of 30 mL can be considered as the limiting volume for this system.

Further analyses on the jet-spun fibers were carried out on two different samples, i.e., 15COC and 30COC. These two concentrations enabled to obtain COC content on CF plies equal to 6.4 wt% and 10.4 wt%, respectively, with a relatively short deposition time, 1.5 h and 3 h. Figure 4 reports the FESEM micrographs of the jet-spun COC microfibers (for the 15COC and 30COC samples) and the distribution of the diameters obtained through dimensional analysis. The jet-spinning process enables to obtain of a high concentration of fibers with a rather narrow size distribution. Moreover, the diameter of the produced fibers is not affected by the deposited volume. In fact, the 15COC mesh is constituted by fibers with a mean diameter of  $0.28 \pm 0.11$   $\mu\text{m}$ , while the 30COC mesh presents a mean diameter of  $0.29 \pm 0.13$   $\mu\text{m}$ .

#### 3.2 | Characterization of the composites

In order to observe the microstructure of the produced laminates, light microscopy (LM) analysis was conducted. Figure 5 reports the LM micrographs of the laminates taken along the longitudinal and transversal cross-sectional directions. EP-CF laminate reports a rather smooth surface in which the epoxy matrix and the CF can clearly be distinguished. In both EP-4COC-CF and EP-8COC-CF samples, it is possible to notice a homogeneous layer of COC microfibers, that does not present voids or defects. The lack of defects and voids proves the fact that the diffusion of the epoxy resin throughout the jet-spun COC mesh and the CF plies was optimal. Furthermore, from the longitudinal cross sections, it is possible to appreciate that, by inserting the COC microfibers on top of the carbon fiber plies, the interlaminar region in between the carbon fiber plies tends to increase.

Table 2 reports the measured density of the prepared laminates. As it is possible to notice, by increasing the amount of COC microfibers in the laminates, the experimental density tends to decrease. A lower density could be reconducted to two different reasons, i.e., the non-complete impregnation of the porous COC mesh by the epoxy resin or, since the composite tends to increase in thickness by increasing the COC content, the pressure difference used to manufacture the composite was not strong enough to eliminate all the air trapped inside the laminates during the hand lay-up process. Nevertheless, the obtained void concentration is acceptable for all the produced laminates. Moreover, by increasing the COC content inside the laminates, a slight decrease in the

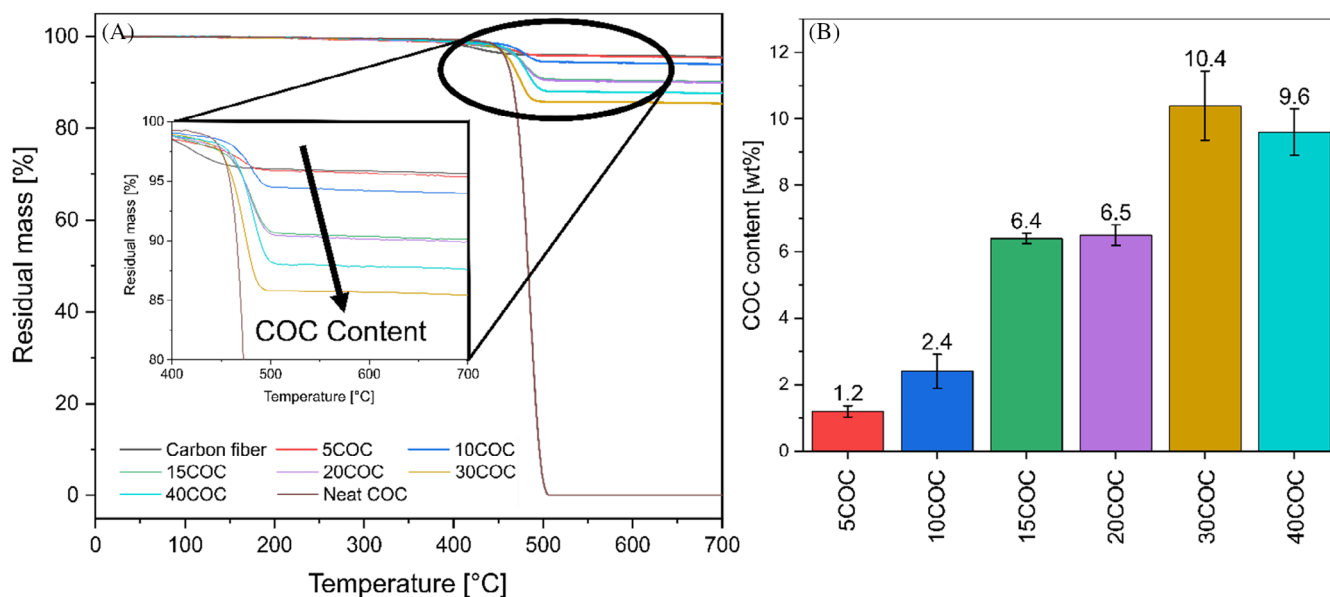


FIGURE 3 (A) Representative TGA thermograms of the carbon fiber fabrics with different concentrations of COC deposited, of neat carbon fiber and neat COC, (B) COC content on carbon fabric as a function of the deposited COC volume.

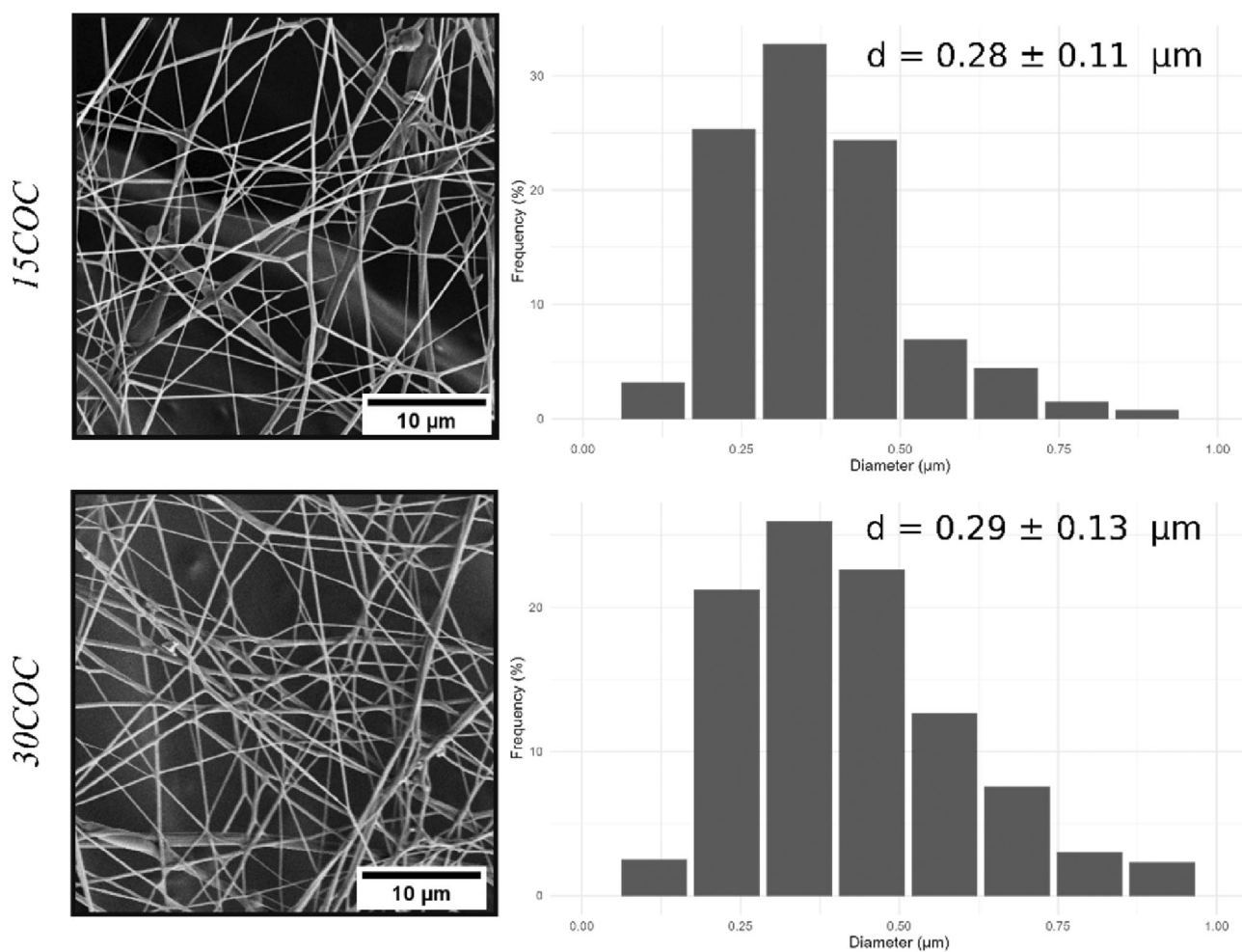


FIGURE 4 SEM micrographs of the jet-spun COC fibers on CF plies and the statistical distribution of the diameter of the fibers.

overall volume fraction of carbon fiber was detected, which could eventually lead to a lowering of the mechanical properties.

In order to obtain information concerning the thermal degradation resistance of the produced laminates, TGA analysis was performed. Figure 6 reports the thermogravimetric curves of neat epoxy resin, of the prepared laminates, and of neat COC granules, while Table 3 summarizes the most important results. By looking at the final residue at 700°C, it is possible to see that epoxy resin has a residue of 8.1%, while COC granules do not have

any residue. COC undergoes thus complete thermal degradation, whereas the laminates only partially degrade because of the presence of carbon fibers which, as reported in Figure 4, have a very limited mass loss. As a consequence, the residual mass at 700°C of all the produced laminates tends to decrease by increasing the COC concentration. Surprisingly, the presence of COC inside the laminates leads to an increase in the  $T_{1\%}$  and  $T_{5\%}$  values, thus suggesting an improved thermal degradation resistance. In fact,  $T_{1\%}$  increases from 247.5°C for EP-CF to 275.0°C for EP-8COC-CF. The reason for this improved thermal resistance lies in the fact that the degradation temperature of the epoxy (360°C) is substantially lower than that of the COC (486°C).

In order to assess the mechanical properties of the prepared laminates, flexural tests were conducted on the six-layered laminates. Representative stress-strain curves are reported in Figure 7A, while Table 4 reports the most important results. In all the tested laminates, brittle fracture occurs and the presence of COC microfibers on the CF plies influences the overall mechanical behavior of the composites. The flexural modulus of EP-4COC-CF and EP-8COC-CF laminates, even slightly lower, is comparable to that of the neat EP-CF. However, a decrease in the flexural strength is observed for both EP-4COC-CF (−32%) and EP-8COC-CF (−26%) laminates compared to the EP-CF composite. Through the addition of COC microfiber on top of CF, the interlaminar region was weakened, and thus the mechanical properties decreased. Furthermore, the decrease in the mechanical properties is partly due to the decrease of the CF content upon the COC insertion (see Table 2). Regarding the flexural strain at break, it is possible to see that it tends to slightly decrease by increasing the COC concentration inside the laminates.

Moreover, the interlaminar resistance was evaluated through short beam shear strength (SBSS) tests. Figure 7B reports representative load-displacement curves obtained from these tests, while the most important results in terms of ILSS values are summarized in Table 4. The ILSS value severely decreases by introducing the COC microfibers, as EP-4COC-CF and EP-8COC-CF laminates report an ILSS drop by 45.7% and 49.7%, respectively, compared to the

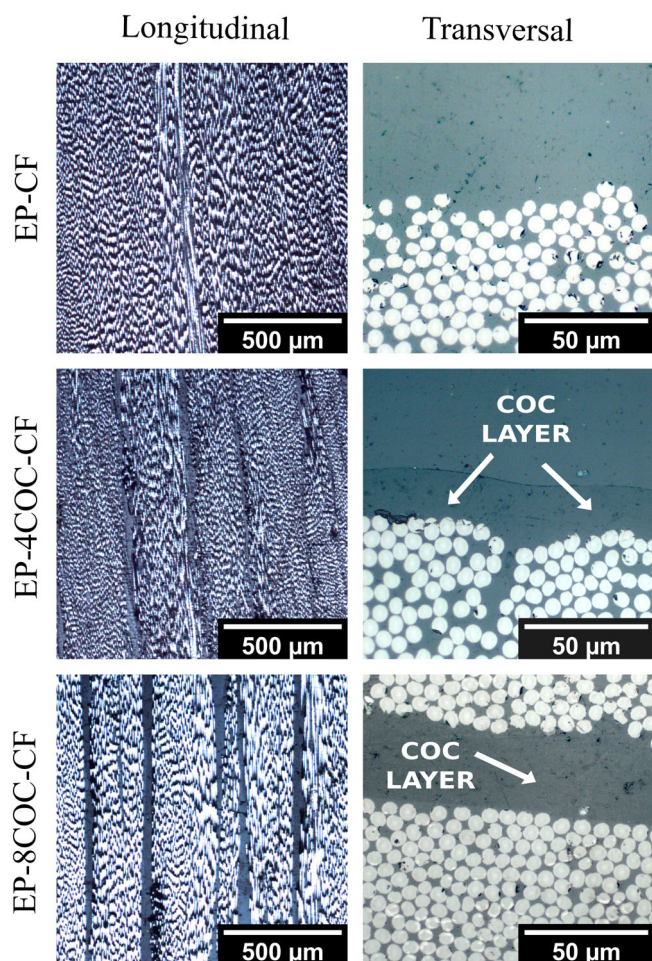


FIGURE 5 Light microscopy micrographs of EP-CF, EP-4COC-CF, and EP-8COC-CF laminates.

TABLE 2 Density and relative composition of the laminates.

	$\rho_{\text{exp}}$ (g/cm <sup>3</sup> )	$\rho_t$ (g/cm <sup>3</sup> )	$\omega_{\text{COC}}$ (wt%)	$\omega_{\text{EP}}$ (wt%)	$\omega_{\text{CF}}$ (wt%)	$V_{\text{COC}}$ (vol%)	$V_{\text{EP}}$ (vol%)	$V_{\text{CF}}$ (vol%)	$V_v$ (vol%)
EP-CF	1.52 ± 0.01	1.57	0.0	26.7	73.3	0.0	34.0	66.0	2.0 ± 0.1
EP-4COC-CF	1.50 ± 0.02	1.53	4.8	25.4	69.8	7.2	31.6	61.2	1.8 ± 0.1
EP-8COC-CF	1.46 ± 0.01	1.49	7.6	27.2	65.2	11.2	33.0	55.8	2.0 ± 0.1

Note:  $\rho_{\text{exp}}$  = experimental density,  $\rho_t$  = theoretical density,  $\omega_{\text{COC}}$  = weight percent of COC,  $\omega_{\text{EP}}$  = weight percent of epoxy resin,  $\omega_{\text{CF}}$  = weight percentage of CF,  $V_{\text{COC}}$  = volume percentage of COC,  $V_{\text{EP}}$  = volume percentage of epoxy resin,  $V_{\text{CF}}$  = volume percentage of CF,  $V_v$  = volume percentage of voids.

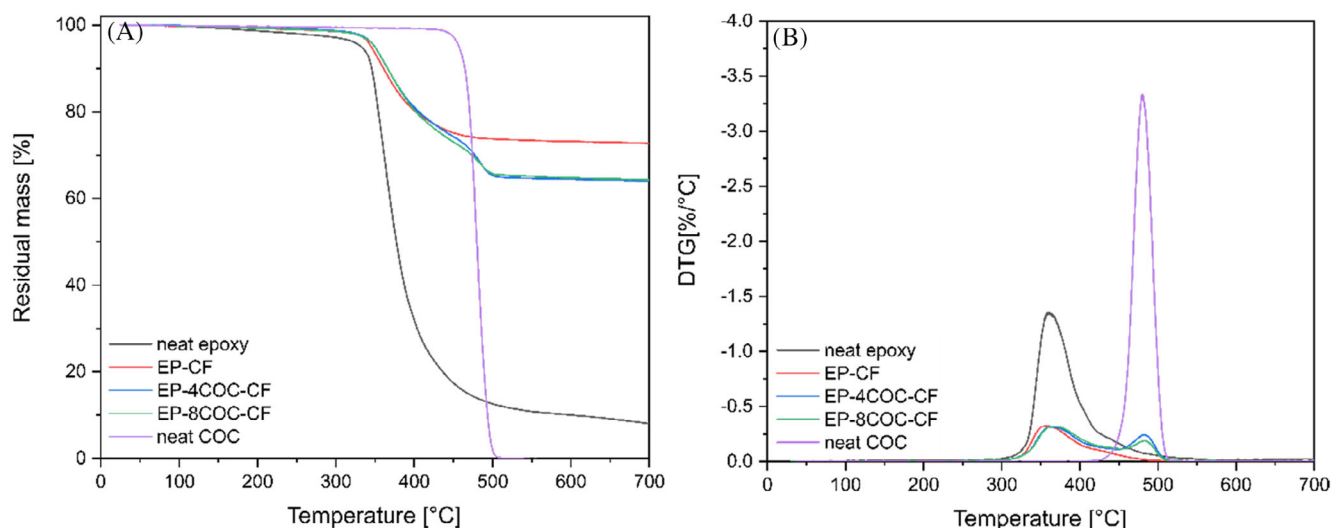


FIGURE 6 TGA analysis of neat epoxy resin, of the prepared laminates, and of neat COC. (A) Residual mass and (B) derivative of the mass loss as a function of the temperature.

	$T_{1\%}$ [°C]	$T_{5\%}$ [°C]	$T_{D\_EP}$ [°C]	$T_{D\_COC}$ [°C]	$m_{700}$ [%]
Neat epoxy	175.5	332.3	360.5	—	8.1
EP-CF	247.3	345.2	356.5	—	72.7
EP-4COC-CF	251.7	349.5	367.5	483.0	64.4
EP-8COC-CF	275.0	349.7	362.5	482.2	64.1
Neat COC	429.2	458.7	—	485.7	0.0

TABLE 3 Results of TGA tests on the prepared laminates, neat epoxy resin and neat COC.

Note:  $T_{1\%}$  = temperature associated with a mass loss of 1%,  $T_{5\%}$  = temperature associated with a mass loss of 5%,  $T_{D\_EP}$  = degradation temperature of epoxy resin,  $T_{D\_COC}$  = degradation temperature of COC, and  $m_{700}$  = residual mass at 700°C.

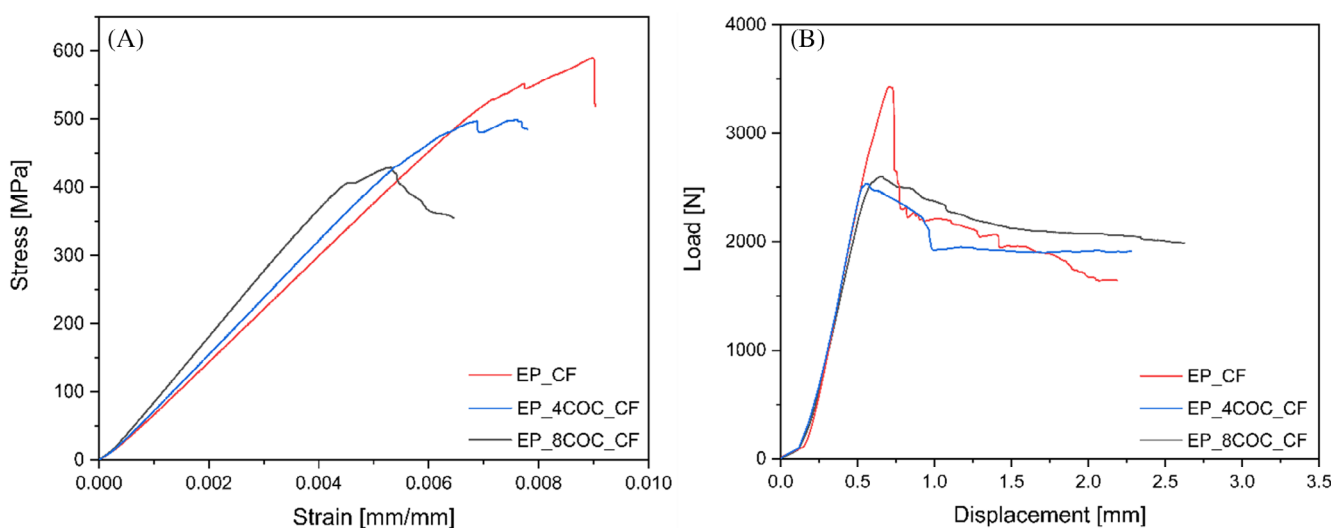


FIGURE 7 (A) Representative stress–strain curves from flexural tests on the prepared composites, (B) representative load–displacement curves from short beam strength tests on the prepared laminates.

EP-CF laminate. This ILSS drop, together with the lower CF content, explains the decrease of the failure properties due to COC mesh introduction. In a previous work of our

group,<sup>37</sup> thin films of COC were inserted in between the CF plies, and in that case, the observed ILSS decay was even harsher (−70% with a COC amount of 10 wt%). This

**TABLE 4** Results of flexural tests and short beam shear strength tests on the prepared laminates.

	Flexural modulus (GPa)	Flexural strength (MPa)	Flexural strain at Break (%)	P <sub>m</sub> (N)	ILSS (MPa)
EP-CF	84.4 ± 5.6	624.9 ± 51.3	0.86 ± 0.13	3427.4 ± 63.8	48.1 ± 0.7
EP-4COC-CF	72.3 ± 4.4	423.8 ± 68.1	0.70 ± 0.15	2534.2 ± 146.0	26.1 ± 1.4
EP-8COC-CF	78.3 ± 6.0	462.2 ± 48.8	0.73 ± 0.05	2544.5 ± 215.8	24.2 ± 2.6

**TABLE 5** Volume and surface electrical resistivity of the prepared laminates.

	Volume resistivity (Ω cm)	Surface resistivity (Ω/sq)
EP-CF	0.34 ± 0.06	2.77 ± 0.47
EP-4COC-CF	0.76 ± 0.15	5.22 ± 0.94
EP-8COC-CF	0.48 ± 0.09	4.22 ± 0.74

means that the approach adopted in the present work, even allowing better retention of the mechanical properties and of the interlaminar adhesion, does not completely solve the problem of the ILSS decrease due to the presence of the healing agent in the interlaminar region. Further studies are needed in order to improve the toughness of the prepared composites and the adhesion between the healing agent and the fibers.

### 3.3 | Evaluation of the healing efficiency

The intrinsic self-healing mechanism selected in this work was based on the softening of COC through a thermal mending process. In order to generate the thermal stimulus through the Joule effect, the evaluation of the resistivity of the produced laminates is fundamental.<sup>47</sup> At this aim, resistivity measurements were carried out by analyzing the voltage–current relationship for each sample.<sup>48</sup> Table 5 reports the results obtained from the resistivity measurements, in terms of volume and surface resistivity. As it is possible to notice, both the volume and surface resistivity tend to slightly increase through the addition of COC microfibers, but they remain in the same order of magnitude. Thus, the obtained values suggest that the utilization of the Joule heating effect is possible as a thermal mending mechanism. It could be also important to underline that these resistivity values are consistent with those found in the literature for similar systems.<sup>49</sup>

The evaluation of the mode I interlaminar fracture toughness was performed both on the virgin and on the healed specimens. Figure 8A reports representative load–displacement curves of the virgin and healed samples, while Figure 8B reports the trends of G<sub>I</sub> as a function of

the delamination length. The most important experimental results are summarized in Table 6. From the load–displacement curves of unhealed laminates (Figure 8A), crack propagation can be noticed. The produced laminates are characterized by a brittle behavior, and thus, each drop in the measured load corresponds to a crack propagation stage.

The G<sub>I</sub> values of the laminates with the COC meshes are slightly lower than that of the neat laminate. In particular, EP-4COC-CF reports G<sub>IC</sub> values 34.7% lower than EP-CF, while EP-8COC-CF has a G<sub>IC</sub> value 22.9% lower than EP-CF. In general, a relatively soft polymeric phase in between the laminates could induce nanofibers bridging effect across the crack plane, therefore improving the toughness of the laminates.<sup>50</sup> In this work, the COC microfibers are too rigid, and it is reasonable to infer that no bridging effect across the crack plane occurs. Furthermore, the lower G<sub>I</sub> of the laminates containing COC could be explained also by the lower interlaminar shear strength (see Table 4 in Paragraph 3.2). Further studies need to be performed in order to enable the nanofiber bridging effect across the crack plane even for rigid polymers.

In order to assess the healing efficiency of the produced laminates, the healed specimens were tested again after the thermal mending process. Figure 8A reports also the load–displacement curves of healed specimens, and it is possible to notice that the fracture is still brittle. The thermal mending process was performed also on neat EP-CF laminate, but it was not repaired at all. It is worth noting that in the healed EP-4COC-CF and EP-8COC-CF laminates a partial restoration of the load-bearing capacity was obtained. It is reasonable to hypothesize that this recovery is due to the addition of COC microfibers, that flow in the crack area upon the thermal treatment. It is widely known that COC can be used as a healing agent and its mending capability has been demonstrated in several works.<sup>33,35,37</sup> The peculiarity of the COC selected in this work is that it is characterized by a low glass transition temperature (T<sub>g</sub> = 65°C). Thus, it tends to soften at relatively low temperatures, and in particular, in the proximity of 100–110°C it is capable to flow inside the cracks. Analyzing the healing efficiency based on the G<sub>I</sub> values, the EP-4COC-CF and EP-8COC-CF laminates report efficiencies of 6.2% and 9.4%, respectively. These

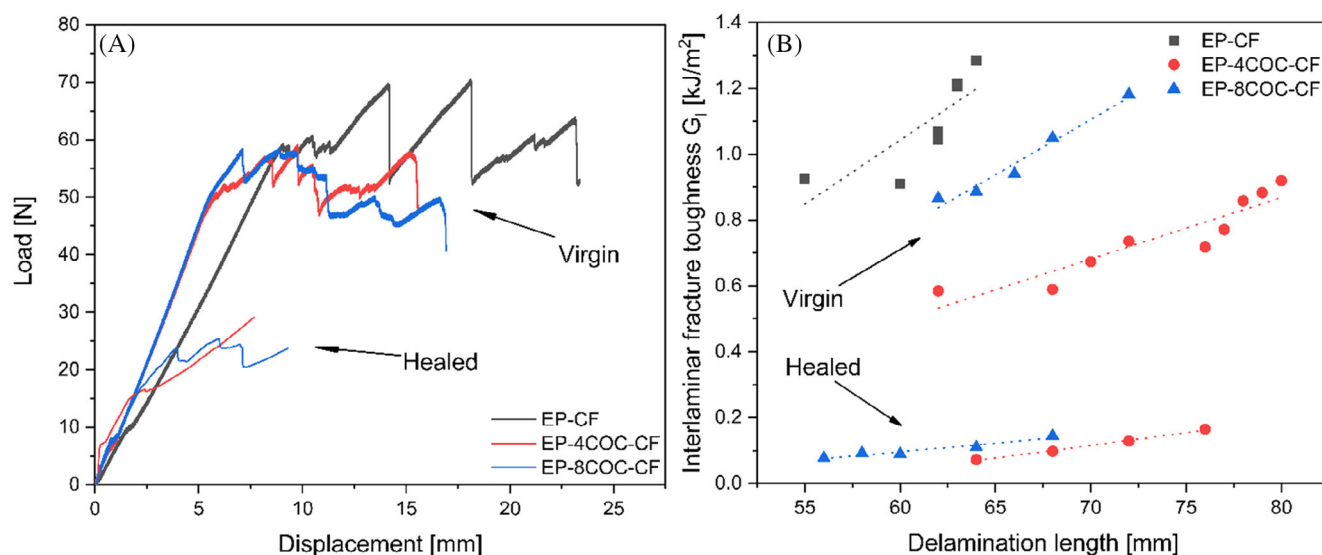


**FIGURE 8** Results of mode I interlaminar fracture toughness tests on the prepared laminates (A) Representative load–displacement curves of virgin and healed samples, (B) representative trend of  $G_I$  as a function of the delamination length in virgin and healed samples.

**TABLE 6** Results of the mode I interlaminar fracture toughness tests on the virgin and healed laminates.

Sample	$P_{MAX}$ [N]		$G_I^{NL}$ [kJ/m <sup>2</sup> ]		Healing efficiency [%]	
	Virgin	Healed	Virgin	Healed	$\eta_{P_{MAX}}$	$\eta_{G_I}$
EP-CF	65.6 ± 6.6	0	1.18 ± 0.18	0	0	0
EP-4COC-CF	55.1 ± 4.8	13.5 ± 2.8	0.77 ± 0.09	0.06 ± 0.02	25.5 ± 5.9	6.2 ± 1.9
EP-8COC-CF	62.8 ± 3.5	20.5 ± 5.5	0.91 ± 0.10	0.09 ± 0.02	33.7 ± 6.7	9.4 ± 1.9

values are rather low, due to the very limited amount of COC in the proximity of the crack and to the low compatibility between COC and epoxy resins. On the hand, considering the healing efficiency as a ratio of the maximum load, it is possible to obtain higher healing efficiencies. In particular, the EP-4COC-CF and EP-8COC-CF laminates show efficiency values of 25.5% and 33.7%, respectively.

In order to better understand the healing mechanism occurring inside the produced laminates, FESEM micrographs of the crack propagation surfaces of virgin and healed samples were taken. Figure 9 reports a comparison between the virgin and healed fracture surfaces of the produced laminates. As it is possible to notice, no appreciable difference can be detected in the EP-CF specimens after the healing process. On the other hand, by inserting the COC microfibers inside the laminates, the fracture surface is completely different. In both EP-4COC-CF and EP-8COC-CF virgin specimens, it is possible to see the COC microfibers forming a dense net. Moreover, it is possible to detect also the traces of the COC microfibers on the cured epoxy, confirming that they retained the pristine morphology after the curing process. The study conducted by Zhang et al.<sup>51</sup> aimed to

investigate the toughening of carbon/epoxy laminates through the use of dissolvable thermoplastic interleaves and electrospun fibers. The authors observed a decrease in fiber diameter with increasing curing temperature and time. Although the dissolution of the fibers was the desired outcome, in several works in the literature there was a risk of converting the microfiber mesh into a thin film if the curing temperature surpassed the melting temperature or the glass transition temperature of the deposited microfibers. In the studies of Yao et al.<sup>34</sup> and Cescato et al.,<sup>35</sup> the curing temperature was deliberately kept below the melting temperature of PCL, in order to avoid the formation of a thin film. However, if the primary objective is to enhance the properties of the epoxy matrix, higher curing temperatures are necessary. For instance, Van der Heijden et al.<sup>52</sup> cured PCL-toughened epoxy at room temperature for 24 hours and subsequently at 80°C for 15 hours to achieve this objective. In the present work, the curing temperature was maintained low enough (60°C) to enable the resin to cure but at the same time assuring that the COC microfiber mesh survived to the curing process.

After the healing process, the COC microfibers softened and tended to aggregate in bigger clusters forming

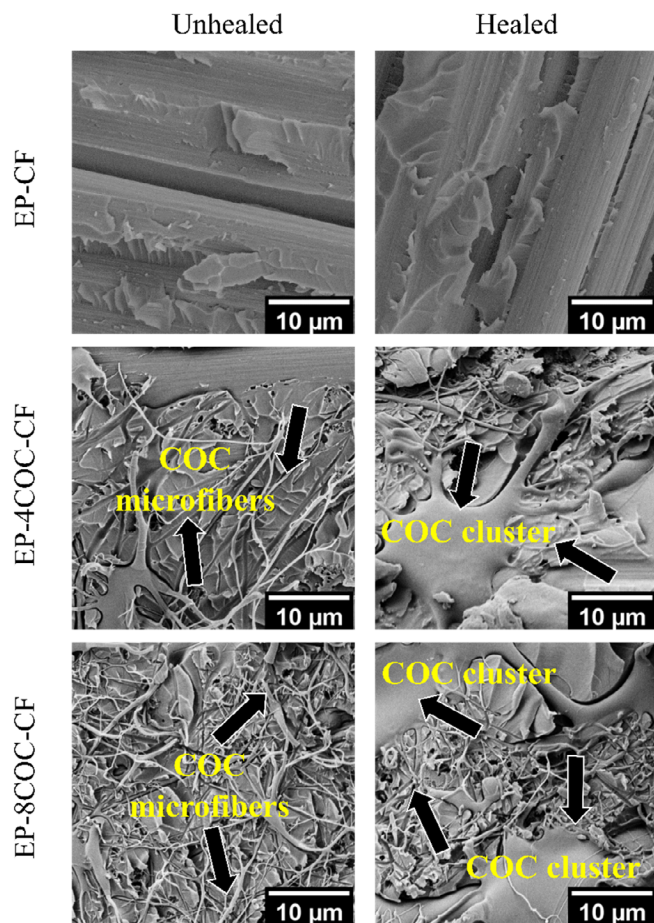


FIGURE 9 SEM micrographs of the fracture surface of the virgin and healed laminates.

thus COC-rich areas and COC-poor areas. This experimental evidence could be of fundamental importance for understanding the reason behind the rather low healing efficiency obtained for these samples. The COC concentrations in the laminates are 4 wt% and 8 wt%, respectively, but the concentration of COC on top of the crack plane is far less. Thus, the COC is capable of filling the cracks but given its limited concentration in the crack plane, complete healing is rather difficult. Furthermore, being the epoxy resin well infiltrated inside the COC microfiber net, even if the COC softens, several microfibers are trapped inside the stiff epoxy matrix, and the diffusion of the softened COC microfibers into the crack zone is therefore hindered. These two aspects explain the limited healing efficiency values observed in the tested laminates.

## 4 | CONCLUSIONS

In this work, COC microfibers were produced through jet-spinning and directly deposited on unidirectional

carbon fiber fabrics to produce multifunctional laminates with intrinsic self-healing properties. At this aim, epoxy/carbon fiber composites with a nominal COC concentration of 4 wt% and 8 wt% were prepared. A comprehensive morphological and thermo-mechanical characterization of the produced laminates was performed. The deposition of COC microfibers led to a slight decrease in the failure properties and in the interlaminar adhesion of the laminates. By exploiting the Joule effect, a temperature rise occurred enabling thus the COC microfibers to soften and heal the fractured surface. The healing efficiency of the produced systems was measured by comparing the  $G_{IC}$  and the  $P_{MAX}$  values of the laminates before and after the thermal mending process. In this way,  $\eta_{GIC}$  and  $\eta_{P_{MAX}}$  values of 9.4% and 33.7% were respectively obtained with a COC content of 8 wt%. Through the analysis of the fracture surfaces, it was possible to notice the agglomeration of the softened COC microfibers in denser regions. However, the deposited COC was not sufficient to provide complete healing, and the majority of the fracture zone did not report COC traces. Further studies will be devoted to improving the healing efficiency of these systems, by enhancing the amount of deposited COC microfibers through the implementation of other technologies, like melt electrowriting.

## ACKNOWLEDGMENTS

Mr. Ciro Polita is gratefully acknowledged for his support to the experimental work.

## DATA AVAILABILITY STATEMENT

Data available on request from the authors

## ORCID

Davide Perin  <https://orcid.org/0000-0002-6248-2012>

Daniele Rigotti  <https://orcid.org/0000-0002-2337-8669>

Alessandro Pegoretti  <https://orcid.org/0000-0001-9641-9735>

## REFERENCES

1. Wang X, Jiang M, Zhou Z, Gou J, Hui D. 3D printing of polymer matrix composites: a review and prospective. *Compos Part B Eng.* 2017;110:442-458.
2. Kangishwar S, Radhika N, Sheik AA, Chavali A, Hariharan S. A comprehensive review on polymer matrix composites: material selection, fabrication, and application. *Polym Bull.* 2023;80:47-87.
3. Kessler MR. Polymer matrix composites: a perspective for a special issue of polymer reviews. *Polym Rev.* 2012;52:229-233.
4. Meng F, Olivetti EA, Zhao Y, Chang JC, Pickering SJ, McKechnie J. Comparing life cycle energy and global warming potential of carbon fiber composite recycling technologies and waste management options. *ACS Sustainable Chem Eng.* 2018;6:9854-9865.

5. Hagnell MK, Åkermo M. The economic and mechanical potential of closed loop material usage and recycling of fibre-reinforced composite materials. *J Clean Prod.* 2019;223:957-968.
6. Saeedifar M, Zarouchas D. Damage characterization of laminated composites using acoustic emission: a review. *Compos Part B Eng.* 2020;195:108039.
7. Guedes RM. Lifetime predictions of polymer matrix composites under constant or monotonic load. *Compos A: Appl Sci Manuf.* 2006;37:703-715.
8. Ansari MTA, Singh KK, Azam MS. Fatigue damage analysis of fiber-reinforced polymer composites—a review. *J Reinf Plast Compos.* 2018;37:636-654.
9. Degriek J, Van Paepegem W. Fatigue damage modeling of fibre-reinforced composite materials: review. *Appl Mech Rev.* 2001;54:279-300.
10. Bao L, Sun Y, Ruan F, Murakami Y, Yu Y. Development of a method for recycling factory waste carbon fiber prepreps and increasing the added value of the collected material. *Polym Compos.* 2023;44:2071-2079.
11. Paolillo S, Bose RK, Santana MH, Grande AM. Intrinsic self-healing epoxies in polymer matrix composites (PMCs) for aerospace applications. *Polymers.* 2021;13:201.
12. Wang Y, Pham DT, Ji C. Self-healing composites: a review. *Cogent Engineering.* 2015;2:1075686.
13. D'Elia E, Eslava S, Miranda M, et al. Autonomous self-healing structural composites with bio-inspired design. *Sci Rep.* 2016;6:25059.
14. Garcia SJ. Effect of polymer architecture on the intrinsic self-healing character of polymers. *Eur Polym J.* 2014;53:118-125.
15. Utrera-Barrios S, Verdejo R, López-Manchado MA, Hernández Santana M. Evolution of self-healing elastomers, from extrinsic to combined intrinsic mechanisms: a review. *Mater Horiz.* 2020;7:2882-2902.
16. Cioffi MOH, Bomfim ASC, Ambrogi V, Advani SG. A review on self-healing polymers and polymer composites for structural applications. *Polym Compos.* 2022;43:7643-7668.
17. An S, Lee MW, Yarin AL, Yoon SS. A review on corrosion-protective extrinsic self-healing: comparison of microcapsule-based systems and those based on core-shell vascular networks. *Chem Eng J.* 2018;344:206-220.
18. Hia IL, Vahedi V, Pasbakhsh P. Self-healing polymer composites: prospects, challenges, and applications. *Polym Rev.* 2016;56:225-261.
19. Gao C, Ruan H, Yang C, Wang F. Investigation on microcapsule self-healing mechanism of polymer matrix composites based on numerical simulation. *Polym Compos.* 2021;42:3619-3631.
20. Lin C, Yuan L, Gu A, Liang G, Wu J. High performance self-healing bismaleimide/diallylbisphenol a/poly(phenylene oxide) microcapsules composites with low temperature processability. *Polym Compos.* 2013;34:335-342.
21. Yang P, Han S, Su J-F, et al. Design of self-healing microcapsules containing bituminous rejuvenator with nano-CaCO<sub>3</sub>/organic composite shell: mechanical properties, thermal stability, and compactability. *Polym Compos.* 2018;39:E1441-E1451.
22. Naga Kumar C, Prabhakar MN, Song J-i. Result of vascular tube design on the curative and mechanical performance of modified carbon fibers/hybrid resin self-healing composites. *Polym Compos.* 2020;41:1913-1924.
23. Urdl K, Kandelbauer A, Kern W, Müller U, Thebault M, Zikulnig-Rusch E. Self-healing of densely crosslinked thermoset polymers—a critical review. *Prog Org Coat.* 2017;104:232-249.
24. White SR, Sottos NR, Geubelle PH, et al. Autonomic healing of polymer composites. *Nature.* 2001;409:794-797.
25. Zhu DY, Rong MZ, Zhang MQ. Self-healing polymeric materials based on microencapsulated healing agents: from design to preparation. *Prog Polym Sci.* 2015;49-50:175-220.
26. Blaiszik BJ, Kramer SLB, Olugebefola SC, Moore JS, Sottos NR, White SR. Self-healing polymers and composites. *Annu Rev Mat Res.* 2010;40:179-211.
27. Guimard NK, Oehlenschlaeger KK, Zhou J, Hilf S, Schmidt FG, Barner-Kowollik C. Current trends in the field of self-healing materials. *Macromol Chem Phys.* 2012;213:131-143.
28. Cohades A, Manfredi E, Plummer CJG, Michaud V. Thermal mending in immiscible poly( $\epsilon$ -caprolactone)/epoxy blends. *Eur Polym J.* 2016;81:114-128.
29. Cohades A, Michaud V. Thermal mending in E-glass reinforced poly( $\epsilon$ -caprolactone)/epoxy blends. *Compos A: Appl Sci Manuf.* 2017;99:129-138.
30. Cohades A, Michaud V. Damage recovery after impact in E-glass reinforced poly( $\epsilon$ -caprolactone)/epoxy blends. *Compos Struct.* 2017;180:439-447.
31. Meure S, Wu DY, Furman S. Polyethylene-co-methacrylic acid healing agents for mendable epoxy resins. *Acta Mater.* 2009;57:4312-4320.
32. Mahmood H, Dorigato A, Pegoretti A. Thermal mending in novel epoxy/cyclic olefin copolymer blends. *Express Polym Lett.* 2020;14:368-383.
33. Dorigato A, Mahmood H, Pegoretti A. Optimization of the thermal mending process in epoxy/cyclic olefin copolymer blends. *J Appl Polym Sci.* 2021;138:49937.
34. Yao Y, Wang J, Lu H, et al. Thermosetting epoxy resin/thermoplastic system with combined shape memory and self-healing properties. *Smart Mater Struct.* 2016;25:015021.
35. Cescato R, Rigotti D, Mahmood H, Dorigato A, Pegoretti A. Thermal mending of electroactive carbon/epoxy laminates using a porous poly( $\epsilon$ -caprolactone) electrospun mesh. *Polymers.* 2021;13:2723.
36. Wang H, Cai H, Chen B, Mao C. Research on core-shell nanofiber self-healing composites for structural applications. *Polym Compos.* 2021;42:3281-3292.
37. Zovi RC, Mahmood H, Dorigato A, Fredi G, Pegoretti A. Cyclic olefin copolymer interleaves for thermally mendable carbon/epoxy laminates. *Molecules.* 2020;25:5347.
38. Bognitzki M, Czado W, Frese T, et al. Nanostructured fibers via electrospinning. *Adv Mater.* 2001;13:70-72.
39. Padron S, Fuentes A, Caruntu D, Lozano K. Experimental study of nanofiber production through forcespinning. *J Appl Phys.* 2013;113:024318.
40. ASTM 5528–21. Standard Test Method for Mode I Interlaminar Fracture Toughness of Unidirectional Fiber-Reinforced Polymer Matrix Composites. Society for Testing and Materials. West Conshohocken, PA 2001.
41. Hotaling NA, Bharti K, Kriel H, Simon CG Jr. DiameterJ: a validated open source nanofiber diameter measurement tool. *Bio-materials.* 2015;61:327-338.
42. ASTM D792-20. Standard Test Methods for Density and Specific Gravity (Relative Density) of Plastics by Displacement.

- Society for Testing and Materials. West Conshohocken, PA 2001.
43. ASTM D790-17. Standard Test Methods for Flexural Properties of Unreinforced and Reinforced Plastics and Electrical Insulating Materials. Society for Testing and Materials. West Conshohocken, PA 2001.
  44. ASTM D2344/D2344-22. Standard Test Method for Short-Beam Strength of Polymer Matrix Composite Materials and their Laminates. Society for Testing and Materials. West Conshohocken, PA 2001.
  45. ASTM D4496-21. Standard Test Method for D-C Resistance or Conductance of Moderately Conductive Materials. Society for Testing and Materials. West Conshohocken, PA 2001.
  46. Karger-Kocsis J. Self-healing properties of epoxy resins with poly ( $\epsilon$ -caprolactone) healing agent. *Polym Bull.* 2016;73:3081-3093.
  47. Junger D, Liebscher M, Zhao J, Mechtcherine V. Joule heating as a smart approach in enhancing early strength development of mineral-impregnated carbon-fibre composites (MCF) made with geopolymer. *Compos A: Appl Sci Manuf.* 2022;153:106750.
  48. Park J-M, Lee S-I, DeVries KL. Nondestructive sensing evaluation of surface modified single-carbon fiber reinforced epoxy composites by electrical resistivity measurement. *Compos Part B Eng.* 2006;37:612-626.
  49. Senis EC, Golosnoy IO, Dulieu-Barton JM, Thomsen OT. Enhancement of the electrical and thermal properties of unidirectional carbon fibre/epoxy laminates through the addition of graphene oxide. *J Mater Sci.* 2019;54:8955-8970.
  50. Daelemans L, Van Der Heijden S, De Baere I, et al. Damage-resistant composites using electrospun nanofibers: a multiscale analysis of the toughening mechanisms. *ACS Appl Mater Interfaces.* 2016;8:11806-11818.
  51. Zhang H, Bharti A, Li Z, du S, Bilotti E, Peijs T. Localized toughening of carbon/epoxy laminates using dissolvable thermoplastic interleaves and electrospun fibres. *Compos A: Appl Sci Manuf.* 2015;79:116-126.
  52. van der Heijden S, Daelemans L, Meireman T, et al. Interlaminar toughening of resin transfer molded laminates by electrospun polycaprolactone structures: effect of the interleave morphology. *Compos Sci Technol.* 2016;136:10-17.

**How to cite this article:** Perin D, Mahmood H, Rigotti D, Dorigato A, Pegoretti A. Novel epoxy/cyclic olefin copolymer/carbon structural composites with electro-activated self-healing properties. *Polym Compos.* 2023;44(8):5173-5187. doi:[10.1002/pc.27482](https://doi.org/10.1002/pc.27482)